Hyperfine Interact (2018) 239:7
https://doi.org/10.1007/s10751-017-1481-z

Influence of sulfur in the precursor mixture on the structural composition of Fe-N-C catalysts

**A. Janßen[1] · I. Martinaiou[1,2] · S. Wagner[2] · N. Weidler[2] ·
A. Shahraei[1,3] · U. I. Kramm[1,2,3]**

Abstract Fe-N-C catalysts were prepared by a new synthesis protocol at 800 °C with subsequent acid leaching. The effect of sulfur was investigated by a systematic study in which the molar S/Fe ratio in the precursor was varied from 0.0 to 2.45. The obtained catalysts were evaluated for their ORR activity in 0.1 M H_2SO_4. In addition, the specific BET surface area was determined from N_2 sorption measurements and structural characterization was made by Mößbauer spectroscopy. Catalysts contain FeN_4 moieties and inorganic iron species. Structure activity correlation indicate a dominance of the ferrous low-spin FeN_4 site for the ORR activity. This is in agreement with previous findings. In addition, the optimum in terms of ORR activity is in the same S/Me range as found for porphyrin-based catalysts. However, in contrast to previous conclusions of an avoidance of iron carbide formation by sulfur addition, a very high S/Fe ratio is required to obtain a catalyst free of iron carbide. Further work is required to identify the parameter that indeed enables inhibition of iron carbide formation.

Keywords Fe-N-C catalysts · Electrocatalysis · Mößbauer spectroscopy · Oxygen reduction reaction (ORR)

This article is part of the Topical Collection on *Proceedings of the International Conference on the Applications of the Mössbauer Effect (ICAME 2017), Saint-Petersburg, Russia, 3–8 September 2017*
Edited by Valentin Semenov

✉ U. I. Kramm
kramm@ese.tu-darmstadt.de

[1] Graduate School of Excellence Energy Science and Engineering, Technische Universität Darmstadt, Otto-Berndt-Str. 3, 64287 Darmstadt, Germany

[2] Department of Materials- and Earth Sciences, Technische Universität Darmstadt, Alarich-Weiss-Str. 2, 64287 Darmstadt, Germany

[3] Department of Chemistry, Technische Universität Darmstadt, Alarich-Weiss-Str. 8, 64287 Darmstadt, Germany

1 Introduction

In proton exchange membrane fuel cells (PEMFC), today platinum supported on carbon (Pt/C) catalysts are the state-of-the-art materials to accelerate the hydrogen oxidation reaction (HOR) and oxygen reduction reaction (ORR). The two half-cell reactions are given in (1) and (2).

$$\text{HOR:} \qquad H_2 \rightarrow 2\,H^+ + 2\,e^- \tag{1}$$

$$\text{ORR:} \qquad O_2 + 4\,H^+ + 4\,e^- \rightarrow 2\,H_2O \tag{2}$$

One major problem that hinders a commercialization of PEMFC is the high cost contributions assigned to Pt/C. About 25% of the overall costs for a PEMFC system to be implemented in cars is attributed to the catalysts [1]! While the HOR is a fast reaction, the ORR is kinetically hindered. That is why about 80% of the used platinum amount are required on the cathodic side for the ORR. Hence, in order to reduce costs it is most effective to reduce the platinum loading or to substitute platinum on the cathode. Higher activity per gram platinum is for instance reached for platinum alloy catalysts, core-shell catalysts, shape controlled nanocrystals or nanoframes of platinum [2]. Nevertheless, in all cases still platinum is used as catalyst, even though it was already defined years ago as a critical raw material by the European Union (EU) [3].

There are different groups of non-precious metal catalysts (NPMC) that showed an activity for the oxygen reduction reaction in acidic environment. So far, Fe-N-C catalysts were the most promising NPMCs [4–7]. In early years Fe-N-C (or in general Me-N-C) were prepared by the pyrolysis of porphyrins or other MeN_4 macrocycles in order to improve ORR activity and stability [8–12]. The today's most active Fe-N-C catalysts are prepared from independent iron, nitrogen and carbon precursors [4, 5, 7]. A major advantage is the possibility to tune iron, nitrogen and carbon contents in the precursor independently from each other.

For porphyrin-based catalysts we were able to show by Mößbauer spectroscopy that only one distinct type of FeN_4 site dominates the ORR activity [13–15]. Later, this type of active site was confirmed for alternative preparation approaches [6, 16–20]. Nevertheless, it should be mentioned that other Fe-based catalysts did not give indication of the presence of FeN_4 sites. Instead, the activity was attributed to iron carbide and/or graphene layers surrounding iron carbide particles [21–23]. This illustrates two important aspects: 1st even though similar precursors might be used the obtained structural composition depends on individual ratios, and pyrolysis conditions (specifically temperature T, time t and pressure p) and 2nd the assignment of ORR activity is complex but required for further optimization of the catalysts.

Zitolo et al. showed for the first time a preparation with the exclusive presence of FeN_4 sites. Catalysts were obtained by a short pyrolysis at 900 °C with low iron content without further conditioning [20]. For another catalyst that indicated at room temperature again only the presence of FeN_4 sites, low-temperature Mößbauer spectroscopy indicated the presence of small fractions of iron oxide nanoparticles [24]. At room temperature these nanoparticles lead to a doublet with Mößbauer parameters that cannot be resolved from the doublet related to the ORR active FeN_4 moiety. Performing an acid leaching avoids the presence of these iron oxide nanoparticles [24]. This underlines the importance of acid-leaching steps in order to enable the removal of acid soluble by-products.

A simple preparation with almost homogeneous composition can be achieved by the oxalate supported pyrolysis of porphyrins with subsequent acid leaching [13]. Performing a second heat-treatment in forming gas (N_2/H_2) with a second acid-leaching enables a high density and exclusive presence of FeN_4 moieties in Fe-N-C as shown recently by X-ray diffraction, X-band electron paramagnetic resonance spectroscopy (EPR) and Mößbauer spectroscopy by us [25].

To the best of our knowledge, the oxalate-supported pyrolysis of porphyrins was the first preparation attempt that worked with an inorganic structure forming agent instead of a carbon support [26]. For cobalt porphyrin pyrolyzed in the presence of iron oxalate and sulfur it was shown that sulfur addition enables significant higher activities in a S/Me range of 0.2 to 0.4 [27]. In a first work, the improved performance was assigned to three aspects: 1st a better solubility of the inorganic by-products that are formed during the pyrolysis, 2nd an enhanced specific BET surface area and 3rd changes in the electronic structure of the surrounding carbon that becomes amorphous by S-addition to the precursor [28]. Also Kiciński et al. recently showed that S-addition can enhance the specific BET surface area [29]. However, further work focusing on the oxalate-supported pyrolysis of iron porphyrin confirmed the improved activity while the surface area was almost identical. Instead, by the combination of in-situ high-temperature X-ray diffraction (HT-XRD), thermogravimetry coupled with mass-spectroscopy (TG-MS) and a detailed characterization of the catalysts we were able to show that without S-addition iron carbide formation coincides with the destruction of FeN_4 sites [30]. Thermodynamic calculations for $S/Fe = 0.37$ confirmed that iron carbide gets only stabilized at temperatures above 810 °C. Without S-addition, in the oxalate-supported pyrolysis iron carbide is formed at about 580 °C [30]. Hence, S-addition enables a simple preparation with relatively homogeneous composition (in terms of FeN_4 sites vs. inorganic iron species) of the catalysts. The improving effect was attributed to the hindrance of supersaturation of iron clusters with carbon by sulfur addition [31]. For this process, sulfur has to adsorb on iron [32].

Based on previous studies, in this work we optimized the ratio of S/Fe in the precursor in order to enable a maximum in current density and the aim of achieving a homogeneous catalyst composition.

2 Experimental part

2.1 Catalyst preparation

For the preparation of the catalysts, 2.85 mM 1,10-phenanthroline (Phen) were mixed with 20.0 mM dicyandiamide (DCDA) and 0.76 mM iron acetate (FeAc) in a mortar until a homogeneous mixture was obtained. In case of sulfur addition, the S-pellets were added to the other precursors and thoroughly mixed. In this work the molar sulfur to iron ratio was varied between $S/Fe = 0.0$ to $S/Fe = 2.45$.

The obtained precursor was filled in a quartz boat and placed in a tube furnace. The overall oven program was run in inert gas atmosphere. The sample was heated with a ramp of 5 $K\ min^{-1}$ up to 300 °C (30 min), 500 °C (30 min) and then finally to 800 °C (60 min). Then the oven was cooled down (<80 °C) before the sample was transferred into 2 M HCl. To accelerate the reaction, the solution was placed for 1 h in an Ultrasonic (US) bath, before it was left overnight. Then the catalyst was filtered and washed with 1.5 l distilled water before the filter cake was dried overnight. The yield was determined from the catalyst weight after drying toward the initial precursor mass (except sulfur). In sample label the S/Fe ratio is indicated as value. For example Fe-N-C_0.82 is the label of the sample prepared with $S/Fe = 0.82$.

2.2 Electrochemistry

In order to investigate the catalytic performance of the electrocatalysts, measurements with a rotating disk electrode (RDE) setup were performed in 0.1 M H_2SO_4. The RDE electrode equipped with a glassy carbon disk ($A_{geo} = 0.1963\ cm^2$) was used as working electrode, a glassy carbon rod and a (Ag/AgCl/3 M KCl) electrode were used as counter and reference electrode. All potential values of this work are given with respect to the standard hydrogen electrode (SHE). In a first step, a catalyst ink was prepared. Therefore, 5 mg of catalyst powder were mixed with 250 μl of a 0.5 wt% Nafion solution in H_2O/EtOH. The suspension was placed in an ultrasonic (US) bath for 15 min, followed by mixing on a Vortexer for 1 min. Both steps were repeated, before the ink preparation was finished with a treatment for about 1 min with a US homogenization needle. 5 μl of this ink were drop casted on the RDE electrode and allowed to dry. The resulting catalyst loading is 0.509 $mg_{cat}\ cm_{geo}^{-2}$.

The overall current in an RDE experiment constitute of the current contributions assigned to oxygen reduction reaction and a capacity current that is attributed to the charging of the electrochemical double layer. The capacity current can be measured by performing the experiments in N_2-saturated electrolyte. In a first place, the catalyst was cycled until steady state was reached in a potential range of 0.0 to 1.2 V(SHE). Then the capacity current was determined by a cathodic linear sweep voltammetry (LSV) with a sweep rate of 10 mV s^{-1}.

Afterwards the electrolyte was saturated with oxygen until a constant value for the open circuit potential was reached (approx. 10–15 min). A LSV in O_2-saturated electrolyte was performed for a rotation speed of 1500 rounds per minute (rpm) with the same conditions as in N_2. After subtracting the capacity current density, the kinetic current density j_{kin} was determined from (3):

$$j^{-1} = j_{kin}^{-1} + j_{diff}^{-1} \tag{3}$$

In this equation, j denotes the capacity corrected overall current density and j_{diff} the diffusion limiting current density. In this work the absolute value of the kinetic current density at a potential of 0.75 V is defined as ORR activity and used for comparison of the different catalysts. An exemplary RDE measurement is given in Fig. 1.

2.3 Physico-chemical characterization

In order to determine the BET surface area of the catalysts, N_2 sorption was measured at 77 K. Previous to the measurements the samples were degassed at 200 °C overnight. Measurements and data analysis were performed with an AUTOSORB instrument from Quantachrome.

Mößbauer spectroscopy was made in transmission mode using a Co/Rh source and a scintillation detector for data acquisition. Calibration of the velocity scale was made with respect to alpha-iron at room temperature. Samples were measured in a velocity range of 6 mm s^{-1}. Lorentzian site analysis was performed to determine Mößbauer parameters. Assignment of iron species was made by comparison to literature data.

3 Results and discussion

3.1 Effect of S/Fe ratio on yield and surface area

As described in the introduction it is the aim to prepare highly active Fe-N-C catalysts with the presence of FeN_4 centers and carbon black, only. Inorganic iron impurities can lead to higher yields and block pores so that less active sites are accessible during ORR.

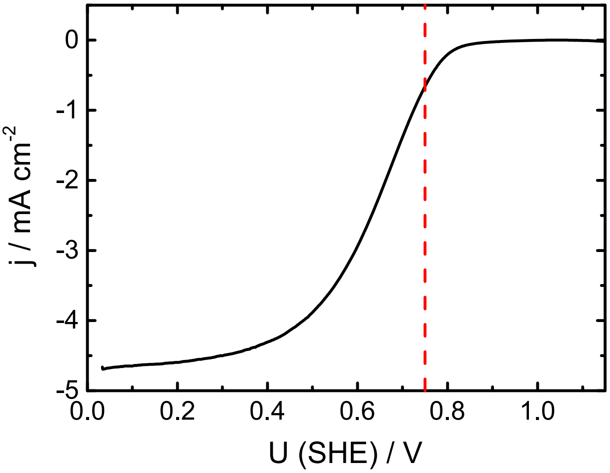

Fig. 1 Exemplary linear sweep voltammetry (LSV) of Fe-N-C_0.82. The potential of 0.75 V is indicated with a dashed line and used for reasons of comparison of different catalysts

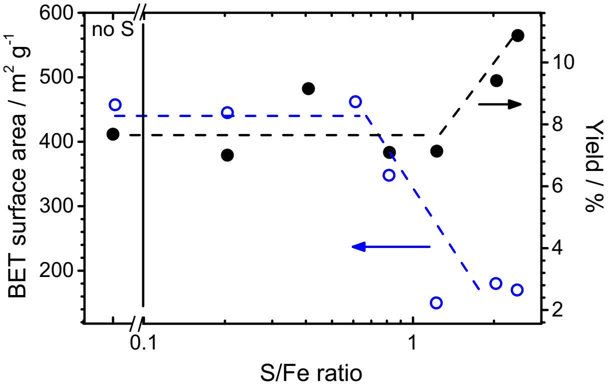

Fig. 2 BET surface area (○) and yield (●) as a function of the S/Fe ratio

Therefore, in Fig. 2 the yield and BET surface area of the different catalysts are given as a function of S/Fe ratio. It can be noted that the yield remains almost constant up to a S/Fe ratio of 1.2. Above this ratio it increases and reaches a maximum of 12%. Contrary, the BET surface area remains constant up to a ratio of S/Fe = 0.6 and starts already to decrease for higher S/Fe ratios. Above S/Fe = 1.0 the BET surface area remains at a low level of <200 m^2 g^{-1}. The trends of yield and BET surface area indicate that most probably inorganic iron species are formed at high S/Fe ratios as it will be confirmed by structural characterization.

3.2 Effect of S/Fe ratio on the oxygen reduction reaction

In order to study the impact of sulfur addition on the electrochemical performance of the catalysts the ORR activity was determined, the obtained values are given in Fig. 3 as a function of S/Fe ratio.

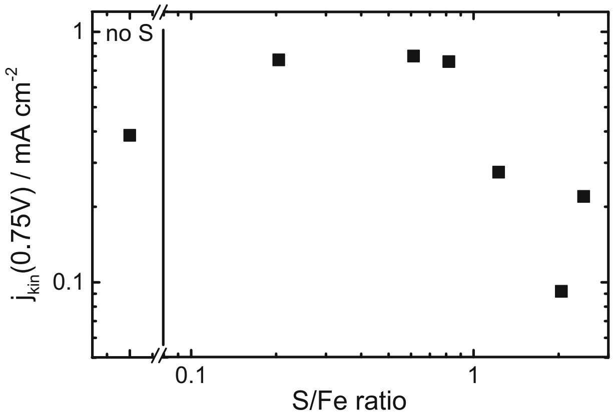

Fig. 3 Kinetic current density at 0.75 V as a function of S/Fe ratio

Induced by sulfur addition, the ORR activity is almost doubled in comparison to the S-free catalyst. Again, above a ratio of S/Fe = 1 the activity drops down and remains at a low level. This drop in ORR activity correlates well with the obtained increases in yield and drop in BET surface area. It can be assumed that the lower ORR activity of the S-free sample might be related to iron carbide formation whereas at high S/Fe ratios iron sulfide species might have been formed. In order to evaluate this statement, the catalysts were checked for the type of iron species present in the catalyst.

3.3 Effect of S/Fe ratio on the structural composition

Mößbauer spectroscopy has proven to be the most suitable technique for the characterization of iron sites in Fe-N-C catalysts. The big advantage is that beside crystalline phases also amorphous structures and in specific FeN_4 sites can be identified. The Mößbauer spectra of the S-free catalyst, with the highest S/Fe ratio and of the most active catalyst (Fe-N-C_0.82) are shown in Fig. 4. The averaged Mößbauer parameters of all three catalysts are summarized in Table 1.

In case of Fe-N-C_0.0 the typical Mößbauer signature of S-free catalysts is obtained. The material is dominated by iron carbide (Sext2), but small lines assigned to alpha-iron are seen as well (Sext1, indicated by arrows) are indicated as well [30, 33]. It is interesting to note, that for the S-free sample the absorption area assigned to FeN_4 sites is significantly larger in comparison to the S-free porphyrin-based Fe-N-C catalysts [30]. On the one hand, this could be attributed to the significant larger nitrogen fraction in the precursor, on the other hand the significant better thermal stability of pyridinic nitrogen in comparison to pyrrolic nitrogen could be at the origin [34].

Fe-N-C_0.0 also contains about 10% of an iron species that was not possible to assign. Fits were performed considering two different approaches. In a first approach a sextet was implemented beside the already known structure. In such a case the isomer shift was indicative of a ferrous high-spin state with a magnetic field of 8.3 T ($X^2 = 2.7$). An even better fit was obtained assuming a further doublet (here labeled D3, compare Table 1, $X^2 = 1.9$). Also here, the isomer shift indicates a high-spin site, with an unusual large quadrupole splitting. In Fig. 4a the model assuming a doublet species was plotted (note: the absorption area of the unknown species accounts in both fit approaches to about 10%).

Fig. 4 Mößbauer spectra for Fe-N-C_0.0 (**a**), Fe-N-C_0.82 (**b**) and Fe-N-C_2.45 (**c**)

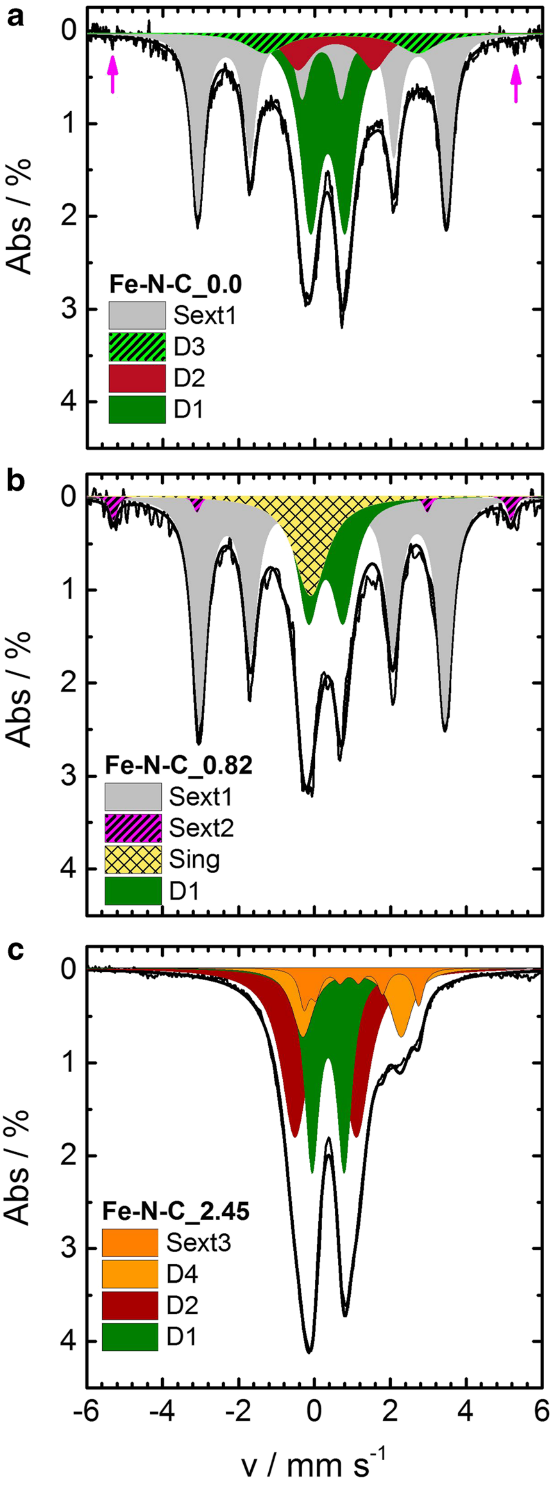

Table 1 Summary of the Mößbauer parameters for the three investigated catalysts and assignment to iron species

	δ_{iso}	ΔE_Q	fwhm	Magn.	Area /%			Assignment
	/mm s^{-1}			Field/T	_0.00	_0.82	_2.45	
Sing	−0.10	–	0.70	–	–	15.1	–	Nano-Iron
D1	0.34	0.90	0.60	–	37.2	22.9	30.4	FeN_4, 2+, LS
D2	0.43	1.81	0.86	–	9.7	–	45.8	FeN_4, 2+, MS
D3	0.71	4.01	1.2 *	–	7.7	–	–	Unknown
D4	0.99	2.59	0.70	–	–	–	15.9	Nano-Fe_3S_4
Sext1	0.19	<0.01	0.42	20.2	45.4	58.6	–	Fe_3C
Sext2	−0.06	–	0.24	32.5	–	3.4	–	α-Fe
Sext3	1.08	0.16	0.32	9.4	–	–	7.9	Nano-Fe_3S_4
					Fe-contents from XPS/wt%			
					0.66	2.41	0.95	

For the most active catalyst Fe-N-C_0.82 the composition was surprising. Even though—based on our previous study [30]—the temperature was in a range where an inhibition of iron carbide formation by sulfur addition was expected, the catalyst still contained iron carbide. So far, iron carbide was only found in S-added catalysts when the temperature exceeded 810 °C [16]. Thermodynamic calculations in our previous work showed that this temperature is the lower limit for the thermodynamic stability of iron carbide in the presence of sulfur. The calculations were made for the S-containing precursor composition of the oxalate-supported pyrolysis [30].

In this work, only for the highest sulfur content, the catalyst Fe-N-C_2.45 was free of iron carbide. In this case, however, two additional iron sites (D4, Sext3) were found. Based on the large isomer shift and due to the presence of excess sulfur, both D4 and Sext3 are assigned to nanoparticles of ferrous iron sulfide [16, 17].

3.4 Correlation of structural composition and ORR activity

As discussed in the introduction the D1 motif was assigned as ORR active site by us and others. In contrast, other groups prepared catalysts even free of the D1 motif but ORR active. Activity was assigned to iron carbide and/or graphene layers surrounding iron carbide structures. Regarding our catalysts, all samples contain the D1 motif, but the Sext1 motif is absent in Fe-N-C_2.45. Therefore, an exclusive ORR activity of the Sext1 motif can be excluded.

From the absorption area of a Mößbauer site and the iron content of the catalyst one can estimate the amount of iron assigned to each motif. We have to assume a homogeneous distribution of iron in our catalysts, as iron contents are only available from X-ray induced photoelectron spectroscopy. The related iron contents were determined for the D1 and Sext1 motif.

In terms of activity, we already concluded from Figs. 1 and 2 that the surface area that is available for ORR catalysis is changing with the variation of S/Fe-content. Therefore, the kinetic current density related to the specific BET surface area is a better measure for a comparison of the three catalysts. Based on the kinetic current density and the catalyst loading on the GC electrode (0.509 $\mathrm{mg_{cat}\ cm_{geo}^{-2}}$) a mass-based kinetic current density can

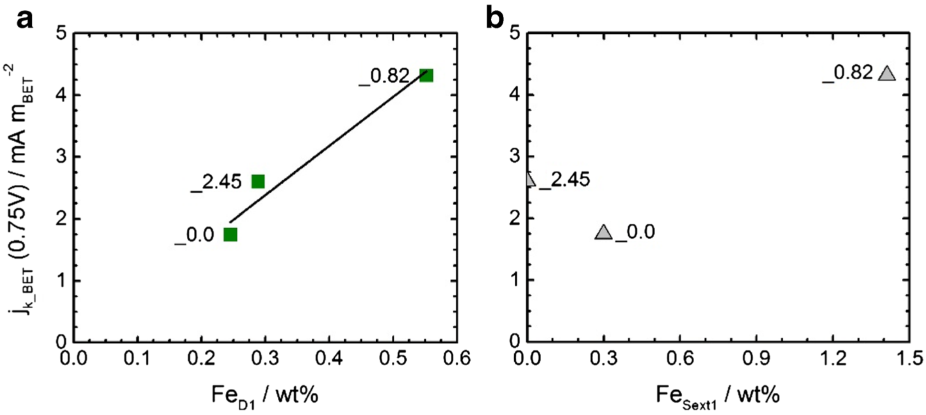

Fig. 5 Correlation of the specific BET surface area related kinetic current density j_{k_BET} with the estimated iron content assigned to D1 (**a**, 🟩) and Sext1 (**b**, ▲)

be determined (in A g_{cat}^{-1}) that can then be related to the specific BET surface area (in m_{BET}^{2} g^{-1}) to get a value j_{k_BET} that gives the kinetic current density in relation to the specific BET surface area (in mA m_{BET}^{-2}). Please note: to avoid confusion between the geometric area of the glassy carbon disk and the BET surface area we implemented the subscript BET for the specific BET surface area.

In Fig. 5 the specific BET surface area related kinetic current density j_{k_BET} is plotted as a function of the iron content assigned to the D1 motif (a) and the Sext1 motif (b). While the correlation of the D1 motif goes straight through zero, there is no trend assigned to the Sext1 motif. This does not necessarily exclude a contribution of iron carbide species to the ORR activity but makes it unlikely. Hence, the observations made for this preparation are in agreement with our previous works.

4 Conclusions

In this work the effect of sulfur was investigated for a new preparation attempt to prepare Fe-N-C catalysts for the oxygen reduction reaction. Several Fe-N-C catalysts were prepared with nominal S/Fe ratios (in precursor) of 0.0 to 2.45. The catalysts without sulfur, with the maximum in activity and with the highest sulfur content were structurally analyzed in detail. In fact, only for the highest S/Fe ratio a catalyst free of iron carbide was obtained, whereas at lower values—and especially also in the range of maximum activity—catalysts contained iron carbide. The results indicate that instead of S/Fe ratio another parameter seems to be of more importance in terms of the possibility of avoiding iron carbide formation.

It is shown that similar to previous conclusions also here, the amount of ORR active D1 sites (ferrous FeN_4, low spin) dominates the catalytic activity of these catalysts. With the aim of achieving a homogeneously composed catalyst with high activity additional work is required to define the parameter that determines whether iron carbide is formed or not.

Acknowledgements Financial support by the German Research Foundation (DFG) for the Graduate School of Excellence Energy Science and Engineering (GSC1070), the Federal Ministry of Education and Research (BMBF) via the projects NUKFER (05K16RD1) and StRedO (03XP0092) is gratefully acknowledged.

References

1. Frank de Bruijn, A., Janssen, G.J.M.: Encycl. Sustain. Sci. Technol. 7694 (2014)
2. Banham, D., Ye, S.: ACS Energy Lett. **2**, 629 (2017)
3. European Commission: Report on critical raw materials for the EU (2014)
4. Proietti, E., Jaouen, F., et al.: Nat. Commun. **2**, 416 (2011)
5. Wu, G., More, K.L., et al.: Science **332**, 443 (2011)
6. Kramm, U.I., Lefèvre, M., et al.: J. Am. Chem. Soc. **136**, 978 (2014)
7. Shui, J., Chen, C., et al.: Proc. Natl. Acad. Sci. USA **112**, 10629 (2015)
8. Bae, I.T., Tryk, D.A., Scherson, D.A.: J. Phys. Chem. B **102**, 4114 (1998)
9. Blomquist, J., Lang, H., et al.: J. Chem. Soc., Faraday Trans. **88**, 2007 (1992)
10. Bouwkamp-Wijnoltz, A.L., Visscher, W., et al.: J. Phys. Chem. B **106**, 12993 (2002)
11. Jahnke, H., Schönborn, M., Zimmermann, G.: Topics Curr. Chem. **61**, 133 (1976)
12. Scherson, D.A., Tanaka, A.A., et al.: Electrochim. Acta **31**, 1247 (1986)
13. Koslowski, U.I., Abs-Wurmbach, I., et al.: J. Phys. Chem. C **112**, 15356 (2008)
14. Kramm, U.I., Abs-Wurmbach, I., et al.: J. Electrochem. Soc. **158**, B69 (2011)
15. Kramm, U.I., Herrmann-Geppert, I., et al.: J. Phys. Chem. C **115**, 23417 (2011)
16. Ferrandon, M., Kropf, A.J., et al.: J. Phys. Chem. C **116**, 16001 (2012)
17. Sahraie, N.R., Kramm, U.I., et al.: Nat. Commun. **6**, 8618 (2015)
18. Zhang, S., Liu, B., Chen, S.: Phys. Chem. Chem. Phys. **15**, 18482 (2013)
19. Zhu, Y., Zhang, B., et al.: Angew. Chem., Int. Ed. **53**, 10673 (2014)
20. Zitolo, A., Goellner, V., et al.: Nat. Mater. **14**, 937 (2015)
21. Hu, Y., Jensen, J.O., et al.: Angew. Chem. Int. Ed. **53**, 3675 (2014)
22. Varnell, J.A., Tse, E.C.M., et al.: Nat. Commun. **7**, 12582 EP (2016)
23. Strickland, K., Miner, E., et al.: Nat. Commun. **6**, 7343 (2015)
24. Sougrati, M.T., Goellner, V., et al.: Catal. Today **262**, 110 (2016)
25. Kramm, U.I., Herrmann-Geppert, I., et al.: J. Am. Chem. Soc. **138**, 635 (2016)
26. Bogdanoff, P., Herrmann, I., et al.: J. New Mater. Electrochem. Syst. **7**, 85 (2004)
27. Herrmann, I.: Doktorarbeit. Freie Universität, Berlin (2005)
28. Herrmann, I., Kramm, U.I., et al.: J. Electrochem. Soc. **156**, B1283 (2009)
29. Kiciński, W., Dembinska, B., et al.: Carbon **116**, 655 (2017)
30. Kramm, U.I., Herrmann-Geppert, I., et al.: J. Mater. Chem. A **2**, 2663 (2014)
31. Marsh, H., Warburton, A.P.: J. Appl. Chem. **20**, 133 (1970)
32. Grabke, H.J., Moszynski, D., et al.: Surf. Interface Anal. **34**, 369 (2002)
33. Greenwood, N.N., Gibb, T.C.: Mössbauer Spectroscopy, 1st edn. Chapman and Hall Ltd., London (1971)
34. Pels, J.R., Kapteijn, F., et al.: Carbon **33**, 1641 (1995)